Structural insights on TRPV5 gating by endogenous modulators

Taylor E.T. Hughes[1], Ruth A. Pumroy[1], Edwin C. Fluck[1], Kevin W. Huynh[2], Amrita Samanta[1], Sudheer Mulugu[1], Z. Hong Zhou[2], Vera Y. Moiseenkova-Bell[1]

[1]Department of Systems Pharmacology and Translational Therapeutics, Perelman School of Medicine, University of Pennsylvania, Philadelphia, Pennsylvania 19104, USA
[2]California NanoSystems Institute, University of California, Los Angeles, California 90095, USA

Corresponding author: V.M.-B. (vmb@pennmedicine.upenn.edu)

ABSTRACT

TRPV5 is a transient receptor potential channel involved in the vital process of calcium homeostasis, specifically at the level of calcium reabsorption in the kidney. TRPV5 is a constitutively open channel and numerous endogenous modulators tightly regulate calcium entry through the TRPV5 channel into the cell. Here we used cryo-electron microscopy (cryo-EM) to investigate the interaction of two such modulators with full-length TRPV5. Both phosphatidylinositol 4,5-bisphosphate ($PI(4,5)P_2$) and calmodulin (CaM) have been reported to directly bind to TRPV5 and activate or inactivate the channel, respectively. Using cryo-EM, we have determined the TRPV5 structure in the presence of dioctanoyl $PI(4,5)P_2$, which revealed the key role annular lipids play in maintaining the channel in a conducting state and highlighted the possibility of a transient interaction between dioctanoyl $PI(4,5)P_2$ and the channel. Additionally, we have uncovered the mechanism of TRPV5 calcium-dependent inactivation, which is mediated by the binding of one CaM molecule per TRPV5 tetramer. This novel mechanism involves the C-lobe of calcium activated CaM physically obscuring the ion conducting pore of TRPV5 by binding to critical tryptophan residues (Trp583) at the intracellular gate of TRPV5. This interaction is initiated by the binding of the CaM C-lobe to the distal C-terminus of TRPV5 which brings CaM in close proximity to the TRPV5 pore. Overall, this investigation has provided insight into the endogenous modulation of TRPV5 which has the potential to guide *in silico* drug discovery and rational drug design for targeted therapeutics for a variety of calcium dependent kidney diseases.

INTRODUCTION

The calcium ion is vital for an array of cellular functions[1]. Calcium homeostasis is tightly controlled in the human body and the kidney regulates this calcium homeostasis by filtration and reabsorption[1]. Around 99% of calcium is reabsorbed by the kidney tubules[1]. The transient receptor potential vanilloid 5 (TRPV5) channel is only expressed in the apical membrane of kidney epithelial cells in the distal convoluted tubule and collecting tubule [2,3]. When open, TRPV5 allows calcium in the urine to flow along a concentration gradient through the channel pore into the cell. This gradient is maintained by the calcium sequestering protein, calbindin, which delivers calcium to active transport proteins at the basolateral membrane of the epithelium, which export the ions into the blood stream[2,3]. Though this mechanism of calcium reabsorption is responsible for only ~15% of total calcium reabsorbed in the kidney, TRPV5 activity is critical for the homeostatic balance of calcium[2,3]. This is exemplified by TRPV5 knock out mice, which have been reported to have systemic calcium imbalance in the form of hypercalciuria and bone mineral loss[2,3]. In humans, single nucleotide polymorphisms in TRPV5 in African-American populations result in a significant increase in calcium reabsorption that is correlated with a lower risk of nephrolithiasis[2,3]. Together, these observations suggest that TRPV5 is a potential drug target for human disorders involving altered calcium homeostasis.

TRPV5 is a constitutively active calcium selective channel and has a variety of endogenous modulators to tightly control its activity in the kidney[2]. Phosphatidylinositol 4,5-bisphosphate ($PI(4,5)P_2$), a lipid found in the plasma membrane, has been shown to directly interact with TRPV5 and to be essential for channel activity[3-5]. Yet, the molecular details of this $PI(4,5)P_2$ interaction with TRPV5 channel is unknown. In addition, to prevent an unnecessary flow of calcium ions into the cell, TRPV5 has been shown to rapidly inactivate through a calcium-dependent mechanism[6]. Calmodulin (CaM), a calcium sensing protein, has been shown to directly interact with the last thirty amino acids of the TRPV5 C-terminus and block its activity[3-6]. While the role of the distal C-terminal binding site is relatively well established in CaM-mediated inactivation of TRPV5[3-6], the binding stoichiometry and the conformational changes that take place as a consequence of the binding of CaM to the channel has been unclear[3-7]. The absence of this information prevents us from further understanding TRPV5 function and regulation in the kidney.

In this study, we used cryo-electron microscopy (cryo-EM) to uncover the molecular mechanisms of TRPV5 gating via endogenous modulators. Investigating TRPV5 modulation with cryo-EM permitted us to gain insight regarding TRPV5 gating and potentially form the basis for rational drug design for the treatment and prevention of hypercalciuria and nephrolithiasis in future studies.

RESULTS

Structures of TRPV5 in the presence of endogenous modulators

TRPV5 is part of the tightly regulated system of calcium homeostasis in the human body[2]. Two endogenous mechanisms of regulation, binding of $PI(4,5)P_2$ or CaM to TRPV5, result in activation or inactivation of the channel[8], respectively. To understand these mechanisms of modulation, we used cryo-EM to determine the structures of detergent solubilized full-length rabbit TRPV5 in the presence of these modulators.

For the structural analysis of $PI(4,5)P_2$ modulation, detergent solubilized full-length rabbit TRPV5 was incubated with 200 µM dioctanoyl (diC_8) $PI(4,5)P_2$, a soluble form of $PI(4,5)P_2$. This concentration is ~3 times the EC_{50} of diC_8 $PI(4,5)P_2$ for TRPV6, and TRPV5 has a slightly higher apparent affinity for diC_8 $PI(4,5)P_2$[9], thus this concentration was expected to result in near saturation of TRPV5 with diC_8 $PI(4,5)P_2$. During the cryo-EM structure determination process, one stable class emerged and was refined to an overall resolution of 3.9 Å (Fig. 1A, Sup. Fig. 1). The vast majority of this TRPV5 cryo-EM map is at high resolution (3-3.5 Å) as side chains are clearly visible in the transmembrane region of the channel (Fig.1A, Sup. Fig. 1, Sup. Fig. 3). This allowed for accurate model building in both the transmembrane domain (TMD) and the ankyrin repeat domain (ARD) (Fig. 1B, Sup. Fig. 1B, Sup. Fig. 3). In spite of the high quality of this map, highly flexible areas such as the very distal C- and N-termini were unable to be resolved. Interestingly, seven non-protein densities per monomer were identified in this cryo-EM map (Fig. 1C). These were attributed to annular lipids that had high enough affinity for TRPV5 to be co-purified with the protein. Unfortunately, even at this resolution we were unable to confidently identify any of these lipids as diC_8 $PI(4,5)P_2$. Therefore, we will conservatively refer to this channel reconstruction as lipid-bound TRPV5.

In order to investigate the mechanism of TRPV5 inactivation by CaM, we incubated detergent solubilized full-length rabbit TRPV5 with activated rat CaM in a 1:20 molar ratio in the presence of 10 mM $CaCl_2$. The stoichiometry of TRPV5 to CaM has been speculated to be between one and four molecules of CaM per tetramer[3-7] and the affinity between CaM and the TRPV5 C-terminus estimated at ~0.3 µM[10], therefore the high molar ratio was used to ensure TRPV5 saturation with CaM. This sample yielded a cryo-EM map at 6.2 Å without applied symmetry (referred to as C1 symmetry) (Fig. 2A, Sup. Fig. 2). In spite of the nominal resolution of this map, it is clear that one single CaM molecule binds to the intracellular section of TRPV5 at the base of the pore (Fig. 2A). To increase the resolution of the CaM-bound TRPV5 map for model building, C4 symmetry was applied, resulting in a 4.9 Å CaM-bound TRPV5 map with the resolution in the TMD ranging between 3.5 Å to 4.5 Å (Fig. 2B, Sup. Fig. 2F). This map allowed for model building in the TMD as well as rigid body refinement of the ARD (Sup. Fig. 2). The TRPV5 model built into the map obtained in the presence of diC_8 $PI(4,5)P_2$ fit into the CaM-bound TRPV5 map generated with C4 symmetry almost perfectly; after real-space refinement in Phenix[11], the RMSD between the two TRPV5 models was only 0.581Å. The model of CaM-bound TRPV5 with C1 symmetry shown in Figure 2C was generated by rigid body refinement of the CaM-bound TRPV5 model with C4 symmetry, the C1 symmetry map was not high enough resolution to refine sidechain placement. CaM, being asymmetrical in both its structure and stoichiometry, was built into the C1 symmetry CaM-bound TRPV5 map (Fig. 2A, Fig. 2C, Sup. Fig. 4A-B). Using the recent NMR model of CaM with a human C-terminal TRPV5 peptide (PDB 5OEO)[7], the N-lobe (Thr6-Met77) and C-lobe (Asp81-Lys149), including the truncated human C-terminal TRPV5 peptide (Ser697-Gly710), were fit independently from each other into the CaM density in the C1 symmetry CaM-bound TRPV5 map using rigid body refinement (Fig. 2C, Sup. Fig. 4A-B). The sequence for human and rat CaM are identical, though the mutations (Glu32Gln/Glu68Gln) made in the NMR structure[7] were returned to the wild type sequence in our model. The human distal TRPV5 C-terminal residues were mutated to rabbit residues in this region, Ser698-Gly711, which shares 93% identity with human TRPV5.

Lipid binding and ion permeation

Of the seven lipids identified in the lipid-bound TRPV5 structure (Fig. 1A, C), four had very strong densities in not only the final map, but also the two half-maps used in the reconstruction which allowed us to confidently differentiate these lipids from noise in our final map (Fig. 3A). Four lipids in similar positions were also found in the CaM-bound TRPV5 structure (Fig. 3B). Since the exact identity of each lipid is unclear they will be referred to as Lipids 1-4, as labeled in Figure 3. Lipid 1 is found in a pocket between the S1 and S2 helices. Lipid 2 is located between the S4 and S5 helices of a single monomer and the S6 helix of the adjacent monomer. This pocket has been previously described as a potential lipid and drug binding site in several TRPV subfamily channels[12-14]. Lipid 3 and 4 occupy areas at the protein lipid interface very near to the extracellular side of the TMD. Based on their placement, it is likely these lipids originated from the outer leaflet of the membrane from which TRPV5 was extracted.

Similarly shaped non-protein densities were also assigned as lipids in a recently reported human TRPV6 cryo-EM structure (Fig. 3C)[14]. Interestingly, while the human TRPV6 structure with these lipids was solved in nanodiscs (Fig. 3C), both lipid-bound TRPV5 and CaM-bound TRPV5 structures were determined in the presence of a mild detergent (Fig. 3A, B). Nanodisc technology is a unique tool that uses variable mixtures of lipids in order to mimic the composition of the plasma and/or intracellular membranes of the cell and has been used to solve the structures of some TRPV subfamily channels in the past[14,15]. Specifically, it was thought that an investigation of lipid interactions with TRPV channels required nanodiscs to accurately visualize lipid binding[14,15]. For rabbit TRPV5, it appears that Lipids 1-4 have such high affinity for these binding sites that they are able to be co-purified regardless of the absence of nanodiscs (Fig. 3).

In addition, Lipids 1-4 in both lipid-bound and CaM-bound TRPV5 structures appear similar in shape and position, indicating that these lipids may be the same in both structures (Fig. 3A, B). Thus, it is unlikely that one of these lipids is diC_8 $PI(4,5)P_2$ in the lipid-bound TRPV5 structure. Nevertheless, at these resolutions we cannot definitively say one way or the other as a wide variety of lipids can be docked into the densities; for example the Lipid 2 density could accommodate diC_8 $PI(4,5)P_2$ and cholesterol (Fig. 3D-F). While the lipid densities in the lipid-bound TRPV5 lack identifiable features, likely due to flexibility of the lipid, the surrounding protein density is very stable and ranges between 3-3.5 Å resolution (Sup. Fig. 1). This has allowed for accurate side chain placement in these areas (Sup. Fig. 3). This is of particular interest as this model is detailed enough for *in silio* drug screening, particularly at the Lipid 1 and Lipid 2 pockets as they could accommodate the binding of other compounds[13]. As mentioned previously, the pocket for Lipid 2 has been identified as the binding site for many small molecules that affect TRPV channels gating[12-14].

The TRPV5 pores revealed here are typical for TRPV family channels and are practically identical for the lipid- and CaM-bound TRPV5, with an RMSD of 0.468Å for the residues in the pore region (Met474-Lys607). In both models, there are three residues that are involved in pore constriction: Asp542, Ile575 and Trp583 (Fig. 4A-B). Unlike the previously published structure of TRPV5[13], there is clear density in the lipid-bound TRPV5 map indicating that the four Asp542 that constitute the highly specific Ca^{2+} selectivity filter are pointing directly into the pore in a similar fashion to the rat TRPV6 crystal structures (Fig. 4, Sup. Fig. 3C)[16,17]. This placement

could facilitate a Ca^{2+} knock-off permeation mechanism as proposed for TRPV6[18]. At the current resolution, it is unclear whether the selectivity filter Asp542 residues in the CaM-bound TRPV5 point directly into the pore or if they point upward, as seen in other TRPV5 and TRPV6 cryo-EM structures (Sup. Fig. 3C)[13,14].

In our lipid- and CaM-bound TRPV5 models, the lower gate appears to consist of Ile575 and Trp583 (Fig. 4A-B). These residues do not constrict the pore to the point of blocking ion translocation, indicating that the lower gate is open (Fig. 4B), as seen in the human TRPV6 cryo-EM structure[14]. Moreover, two probable ion densities occupy the selectivity filter and lower gate in the lipid-bound TRPV5 channel (Fig. 4C). Thus, suggesting that the pore of the lipid-bound TRPV5 structure is in a conducting conformation and co-purified tightly bound lipids play a key role in keeping TRPV5 in constitutively open state.

TRPV5 inhibition by calmodulin

From our C1 symmetry CaM-bound TRPV5 cryo-EM map it is clear that the TRPV5-CaM complex adopts a stoichiometry of one tetramer of TRPV5 to one molecule of CaM (Fig. 2A). The CaM cryo-EM density consists of two lobes, an upper lobe sitting at the intracellular gate of the pore and a lower lobe interacting with the TRPV5 ankyrin repeats (Sup. Fig. 4A). The density for CaM contains tubular density that allowed for the manual fit of CaM helices and rigid body refinement of the individual lobes of the previously published NMR structure of CaM bound to the C-terminus of TRPV5 (PDB 5OEO)[7] (Sup. Fig. 4B). The N- and C-lobes of CaM have very similar structural organization (Fig. 5A), so it was not possible, based on modeling only CaM, to determine whether the CaM N- or C-lobe was positioned in the upper lobe of density at the bottom of the TRPV5 pore (Fig. 5, Sup. Fig. 4A). However, there was extra density in the upper lobe that could not be attributed to CaM (Sup. Fig. 4B). This density was in the same position relative to that lobe as the helical portion of the TRPV5 C-terminus relative to the CaM C-lobe in the NMR structure[7]. Therefore, we surmise that the CaM upper lobe is the C-lobe in our cryo-EM structure and we have included the rabbit C-terminal TRPV5 helix, comprising residues Ser698-Gly711, in our model (Fig. 5). The density for the CaM lower lobe, modelled as the N-lobe, is weaker and sparser than the density for the C-lobe, indicating that the N-lobe may be more flexible or bound weakly to TRPV5 (Sup. Fig. 4B). Interestingly, at this resolution we clearly see density for two calcium ions in the C-lobe (Fig. 5B), while the N-lobe does not have enough detail to place any calcium ions (Sup. Fig. 4B).

Based on this CaM model, as well as data available in the literature[3-8], we can postulate a mechanism of action for calcium-dependent inactivation of TRPV5 by CaM. The increase in calcium ion concentration at the intracellular gate of the TRPV5 channel recruits one molecule of CaM. This recruitment likely occurs via the high affinity interaction between the Ca^{2+}-bound CaM C-lobe and the distal C-terminus of TRPV5[7]. The C-lobe of CaM then obscures the flow of ions through the TRPV5 pore by inserting a loop, comprising residues Leu113-Asp119, into the bottom of the TRPV5 pore. This CaM C-lobe loop likely interacts with the Trp583 residues at the base of the TRPV5 pore (Fig. 5A). A CaM C-lobe helix, comprising residues Ser102-Asn112, interacts with a single Gln587, which is located in the TRP domain of the channel (Fig. 5A). These interactions are supported in the cryo-EM C1 symmetry density map of CaM-bound TRPV5, where there are strong connections in these regions (Sup Fig. 4C). Additionally, it appears that an N-lobe helix of CaM (Pro44-Asp59)

binds between ankyrin repeat 2 (AR2) and ankyrin repeat 3 (AR3) of a single TRPV5 monomer, which could act to stabilize this interaction (Fig 5A).

CONCLUSION

Here we have presented two structures of TRPV5, one in the presence of endogenous lipids that are likely to be involved in maintaining the structure of TRPV5 in a constitutively open state and one bound to its endogenous inhibitor, calmodulin. The high-resolution, lipid-bound TRPV5 has allowed for more accurate model building of TRPV5 than available previously[13]. This structure also identified the binding pockets for several high affinity lipids. These binding pockets have the potential to be drugable areas of the TRPV5 channel as they are both membrane and solvent accessible and are in contact with regions that have been reported to be able to transmit conformational rearrangements to the pore in other TRPV family channels[12-14].

The CaM-bound structure, though at lower nominal resolution, has provided the first insight as to how TRPV5 is modulated by CaM. It is clear that the binding of a single CaM molecule completely obstructs the intracellular side of the pore, effectively blocking ion permeation (Fig. 6). This study also showed that while CaM binds to the predicted areas in the C-terminus of TRPV5, it also directly interacts with the ankyrin repeat domain and the TRP domain of the channel (Fig. 6). These two structures taken together also provide additional evidence for the static nature of some TRPV subfamily channels[12,14]. The minimal movement between the two structures imply that large conformational changes in the upper and lower gates of TRPV5 may not be necessary for effective endogenous inhibition.

It is possible that the high affinity of the structural lipids identified in the lipid bound structure are bound too tightly in this non-native environment to have allowed for diC_8 $PI(4,5)P_2$ binding. In the future, studies can be undertaken to solve the structure of TRPV5 in the presence of higher concentrations of diC_8 $PI(4,5)P_2$. Additionally, mutations of TRPV5 have been reported to increase the affinity of TRPV5 to $PI(4,5)P_2$ and solving the structure of these mutants in the presence of diC_8 $PI(4,5)P_2$ may allow for a clearer picture of TRPV5 gating by $PI(4,5)P_2$.

Overall, our structural studies have provided novel molecular insights into the endogenous modulation of TRPV5 that could guide novel therapeutics design for a variety of calcium dependent kidney diseases.

METHODS

Expression and purification of TRPV5

Full length rabbit TRPV5 was expressed as reported previously[13]. In short, full length rabbit TRPV5 was expressed with a 1D4 affinity tag in S. cerevisiae[19,20]. The membranes were lysed and harvested using a M-110Y microfluidizer and ultracentrifugation. TRPV5 was purified using previously published methods[13]. Briefly, membranes containing TRPV5 were solubilized in Buffer A (150mM NaCl, 2mM TCEP, 1mM PMSF, 20 mM HEPES pH8, 10% glycerol and 0.87 mM LMNG). Non-soluble material was removed via ultracentrifugation. Detergent solubilized TRPV5 was then purified using CnBr-activated Sepharose 4B beads conjugated to 1D4 specific antibodies. The beads were washed with Buffer B (150mM NaCl, 2mM TCEP, 20 mM HEPES pH8, and 0.064 mM DMNG) and TRPV5 was eluted using Buffer B with the addition of 3 mg/mL 1D4 peptide.

The sample involved in the reconstruction of lipid-bound TRPV5 was then subjected to size exclusion chromatography (Superose 6, GE Healthcare) in Buffer B. This sample was concentrated to ~2.5mg/mL and incubated with soluble diC_8 $PI(4,5)P_2$ (dioctanoyl Phosphatidylinositol 4,5-bisphosphate) at a final concentration of 200μM for 30 minutes prior to vitrification.

The TRPV5 sample used for the reconstruction of CaM-bound TRPV5 was incubated for 1 hr with 10mM CaCl and purified rat CaM (a gift from the Dr. Zhang lab at Thomas Jefferson University purified as previously published[21]) at a molar ratio of 1:20 (TRPV5 tetramer:CaM). The TRPV5-CaM mixture was then further purified using size exclusion chromatography (Superose 6, GE Healthcare) in Buffer B. The peak containing CaM-bound TRPV5 was concentrated to ~3mg/mL.

Cryo-EM data acquisition

For both samples, fluorinated Fos-Choline-8 was added to the concentrated protein to a final concentration of 3mM immediately prior to vitrification. Samples were double blotted on 200 mesh Quantifoil 1.2/1.3 grids (Quantifoil Micro Tools) with 3.5μL per blot and plunge frozen in liquid ethane using a Vitrobot (FEI). Grids containing TRPV5 and diC_8 $PI(4,5)P_2$ were imaged with a 300kV FEI Titan Krios microscope equipped with a Gatan K2 Summit direct detector camera. Super resolution movies (50 frames) were captured for 10 sec each with one frame collected every 0.2 sec at a nominal magnification of 45,455x. The resultant pixel size and dose rate were 0.55 Å/pix and ~8 electrons/pix/sec, respectively. Images were collected in a defocus range between 1.0-2.5μm under focus in an automated fashion using Leginon software[22].

Grids containing CaM-bound TRPV5 were imaged using a 300kV FEI Titan Krios microscope equipped with a Falcon 3 direct detector camera. Movies (60 frames) were acquired in counting mode at a magnification of 59,000x resulting in a pixel size of 1.14Å/pix. Images were collected automatically using EPU software (Thermo Fisher Co.) within a defocus range of 1.0-2.5μm under focus[23].

Image processing

Lipid-bound TRPV5

MotionCor2[24] was used to correct for beam induced motion and to bin the images to a final pixel size of 1.10Å, producing both summed and dose weighted micrographs. CTF estimation of the summed micrographs was preformed using Gctf[25]. All other image processing was performed using RELION on the dose weighted micrographs unless otherwise mentioned[26,27]. Approximately 2,500 particles were picked manually from 3,889 micrographs and sorted into 2D classes. The best of these classes were used as templates for autopicking. After autopicking, 2D classification was used to remove false positives and suboptimal particles. The remaining ~241,000 particles were reconstructed into a single electron density map with C4 symmetry using the 3D auto-refine option in RELION followed by 3D classification into 8 classes without assigning angles to the particles. The initial model used for 3D refinement and classification was produced by applying a low-pass filter of 60Å to the previously published TRPV5 cryo-EM structure[13]. The best class by manual inspection underwent multiple rounds of 3D refinement followed by 3D classification until the best 26,000 particles were able to be reconstructed into 4.4Å map. The mask used for this reconstruction was

created from the original 3D auto-refinement of ~241,000 particles adjusted to a threshold of 0.005, lowpass filtered to 15Å and a soft edge of 5 pixels was applied. A separate dataset collected under the same conditions on grids prepared at the same time as the sample above produced 3,062 additional micrographs. The same methods as above were implemented and resulted in a map containing ~19,000 particles that was reconstructed to 4.2Å. These particles were then combined using the JoinStar command in Relion to produce a particle set of ~45,000 particles that were refined to 4.1Å in RELION. A b-factor of -174 was then applied to the unsharpened map using Bfactor software and the final resolution of 3.9Å was determined using rmeasure software[28,29]. Local resolutions were estimated using the RESMAP software[30].

CaM-bound TRPV5

For the CaM-bound dataset, MotionCorr2[24] was used without gain correction and without binning to produce both summed and dose weighted micrographs with a final pixel size of 1.14Å. CTF estimation of the summed micrographs was preformed using Gctf[25]. Autopicking was performed on the dose weighted micrographs in cisTEM[31] resulting in 406,838 particles from 1,524 micrographs. These particles were then exported to RELION for all subsequent data processing. The particles were 2D classified into 200 classes to remove false positives and suboptimal particles. These particles were then 3D classified into 6 classes without applied symmetry. The best class by visual inspection contained ~64,000 particles and was auto-refined to 6.4Å. The initial model used for 3D refinement and classification was produced by applying a low-pass filter of 60Å to the previously published TRPV5 cryo-EM structure[13]. The mask used for that refinement was created from the C1 symmetry class containing those ~64,000 particles adjusted to a threshold of 10Å, lowpass filtered to 10Å and a soft edge of 5 pixels was applied. These particles were then subjected to another round of 3D classification without assigning angles using a partial mask only containing the TMD region of the protein. This mask was created from the ~64,000 particle mask using the Chimera Volume Eraser tool[32] to remove all density except the TMD. The best class by manual inspection contained ~19,000 particles and was able to be reconstructed with C1 symmetry to 6.4Å and 4.86Å with C4 symmetry. A soft mask of the whole complex created from the original C1 reconstruction of ~64,000 particles was applied for postprocessing which resulted in at C1 6.2Å map based on the 0.143 cut-off criterion. A soft mask of the auto-refined C4 reconstruction created with similar parameters was applied to the C4 reconstruction for postprocessing resulting in a 4.86Å map based on the 0.143 cut-off criterion. Local resolutions were estimated using the RESMAP software[30].

Model Building

The previously published model of TRPV5 bound to econazole (PDB 6B5V)[13] was used as an initial model and docked to the cryo-EM map of lipid-bound TRPV5. The model was manually adjusted in Coot[33] and refined against one of two unfiltered half maps using phenix.real_space_refinement[11]. The lipid-bound TRPV5 map was docked into the CaM-bound TRPV5 map generated with C4 symmetry and manually adjusted and refined as before. The TRPV5 model generated in C4 was docked into the C1 map by rigid body fit in Coot[33]. To model CaM into the extra density in the C1 symmetry map, the N-lobe and C-lobe (including the TRPV5 C-terminal peptide) of state 01 of PDB 5OEO[7] were separated and independently fit to the map by hand in

Chimera[32] and then rigid body fit in Coot[33]. Due to the low resolution, the combined TRPV5 and CaM models were refined with only rigid body refinement. The final models were randomized in PHENIX[11] by 0.5Å and Chimera[32] was used to generate a map of those models. EMAN2 was used to generate FSC curves between the two half maps and the summed map for each model. The pore radii were generated using HOLE[34]. Figures were made in Pymol[35] and Chimera[32].

REFERENCES

1 Zhou, Y. & Greka, A. Calcium-permeable ion channels in the kidney. *Am J Physiol Renal Physiol* **310**, F1157-1167, doi:10.1152/ajprenal.00117.2016 (2016).

2 Na, T. & Peng, J. B. TRPV5: a Ca(2+) channel for the fine-tuning of Ca(2+) reabsorption. *Handb Exp Pharmacol* **222**, 321-357, doi:10.1007/978-3-642-54215-2_13 (2014).

3 van Goor, M. K. C., Hoenderop, J. G. J. & van der Wijst, J. TRP channels in calcium homeostasis: from hormonal control to structure-function relationship of TRPV5 and TRPV6. *Biochim Biophys Acta* **1864**, 883-893, doi:10.1016/j.bbamcr.2016.11.027 (2017).

4 van der Wijst, J. *et al.* A Gate Hinge Controls the Epithelial Calcium Channel TRPV5. *Sci Rep* **7**, 45489, doi:10.1038/srep45489 (2017).

5 Rohacs, T., Lopes, C. M., Michailidis, I. & Logothetis, D. E. PI(4,5)P2 regulates the activation and desensitization of TRPM8 channels through the TRP domain. *Nat Neurosci* **8**, 626-634, doi:10.1038/nn1451 (2005).

6 Nilius, B. *et al.* The carboxyl terminus of the epithelial Ca(2+) channel ECaC1 is involved in Ca(2+)-dependent inactivation. *Pflugers Arch* **445**, 584-588, doi:10.1007/s00424-002-0923-9 (2003).

7 Bokhovchuk, F. M. *et al.* The Structural Basis of Calcium-Dependent Inactivation of the Transient Receptor Potential Vanilloid 5 Channel. *Biochemistry* **57**, 2623-2635, doi:10.1021/acs.biochem.7b01287 (2018).

8 Cao, C., Zakharian, E., Borbiro, I. & Rohacs, T. Interplay between calmodulin and phosphatidylinositol 4,5-bisphosphate in Ca2+-induced inactivation of transient receptor potential vanilloid 6 channels. *J Biol Chem* **288**, 5278-5290, doi:10.1074/jbc.M112.409482 (2013).

9 Velisetty, P. *et al.* A molecular determinant of phosphoinositide affinity in mammalian TRPV channels. *Sci Rep* **6**, 27652, doi:10.1038/srep27652 (2016).

10 Holakovska, B., Grycova, L., Bily, J. & Teisinger, J. Characterization of calmodulin binding domains in TRPV2 and TRPV5 C-tails. *Amino Acids* **40**, 741-748, doi:10.1007/s00726-010-0712-2 (2011).

11 Adams, P. D. *et al.* PHENIX: a comprehensive Python-based system for macromolecular structure solution. *Acta Crystallogr D Biol Crystallogr* **66**, 213-221, doi:10.1107/S0907444909052925 (2010).

12 Gao, Y., Cao, E., Julius, D. & Cheng, Y. TRPV1 structures in nanodiscs reveal mechanisms of ligand and lipid action. *Nature* **534**, 347-351, doi:10.1038/nature17964 (2016).

13 Hughes, T. E. T. *et al.* Structural basis of TRPV5 channel inhibition by econazole revealed by cryo-EM. *Nat Struct Mol Biol* **25**, 53-60, doi:10.1038/s41594-017-0009-1 (2018).

14 McGoldrick, L. L. *et al.* Opening of the human epithelial calcium channel TRPV6. *Nature* **553**, 233-237, doi:10.1038/nature25182 (2018).

15 Grinkova, Y. V., Denisov, I. G. & Sligar, S. G. Engineering extended membrane scaffold proteins for self-assembly of soluble nanoscale lipid bilayers. *Protein Eng Des Sel* **23**, 843-848, doi:10.1093/protein/gzq060 (2010).

16 Saotome, K., Singh, A. K., Yelshanskaya, M. V. & Sobolevsky, A. I. Crystal structure of the epithelial calcium channel TRPV6. *Nature* **534**, 506-511, doi:10.1038/nature17975 (2016).

17 Singh, A. K., Saotome, K. & Sobolevsky, A. I. Swapping of transmembrane domains in the epithelial calcium channel TRPV6. *Sci Rep* **7**, 10669, doi:10.1038/s41598-017-10993-9 (2017).

18 Sakipov, S., Sobolevsky, A. I. & Kurnikova, M. G. Ion Permeation Mechanism in Epithelial Calcium Channel TRVP6. *Scientific Reports* **8**, 5715, doi:10.1038/s41598-018-23972-5 (2018).

19 Moiseenkova, V. Y., Hellmich, H. L. & Christensen, B. N. Overexpression and purification of the vanilloid receptor in yeast (Saccharomyces cerevisiae). *Biochem Biophys Res Commun* **310**, 196-201 (2003).

20 Moiseenkova-Bell, V. Y., Stanciu, L. A., Serysheva, II, Tobe, B. J. & Wensel, T. G. Structure of TRPV1 channel revealed by electron cryomicroscopy. *Proc Natl Acad Sci U S A* **105**, 7451-7455, doi:10.1073/pnas.0711835105 (2008).
21 Zhang, M. *et al.* Selective phosphorylation modulates the PIP2 sensitivity of the CaM-SK channel complex. *Nat Chem Biol* **10**, 753-759, doi:10.1038/nchembio.1592 (2014).
22 Potter, C. S. *et al.* Leginon: a system for fully automated acquisition of 1000 electron micrographs a day. *Ultramicroscopy* **77**, 153-161 (1999).
23 Tan, Y. Z., Cheng, A., Potter, C. S. & Carragher, B. Automated data collection in single particle electron microscopy. *Microscopy (Oxf)* **65**, 43-56, doi:10.1093/jmicro/dfv369 (2016).
24 Zheng, S. Q. *et al.* MotionCor2: anisotropic correction of beam-induced motion for improved cryo-electron microscopy. *Nat Methods* **14**, 331-332, doi:10.1038/nmeth.4193 (2017).
25 Zhang, K. Gctf: Real-time CTF determination and correction. *J Struct Biol* **193**, 1-12, doi:10.1016/j.jsb.2015.11.003 (2016).
26 Scheres, S. H. RELION: implementation of a Bayesian approach to cryo-EM structure determination. *J Struct Biol* **180**, 519-530, doi:10.1016/j.jsb.2012.09.006 (2012).
27 Scheres, S. H. Processing of Structurally Heterogeneous Cryo-EM Data in RELION. *Methods Enzymol* **579**, 125-157, doi:10.1016/bs.mie.2016.04.012 (2016).
28 Grigorieff, N. Resolution measurement in structures derived from single particles. *Acta Crystallogr D Biol Crystallogr* **56**, 1270-1277 (2000).
29 Sousa, D. & Grigorieff, N. Ab initio resolution measurement for single particle structures. *J Struct Biol* **157**, 201-210, doi:10.1016/j.jsb.2006.08.003 (2007).
30 Kucukelbir, A., Sigworth, F. J. & Tagare, H. D. Quantifying the local resolution of cryo-EM density maps. *Nat Methods* **11**, 63-65, doi:10.1038/nmeth.2727 (2014).
31 Grant, T., Rohou, A. & Grigorieff, N. cisTEM, user-friendly software for single-particle image processing. *Elife* **7**, doi:10.7554/eLife.35383 (2018).
32 Pettersen, E. F. *et al.* UCSF Chimera--a visualization system for exploratory research and analysis. *J Comput Chem* **25**, 1605-1612, doi:10.1002/jcc.20084 (2004).
33 Emsley, P. & Cowtan, K. Coot: model-building tools for molecular graphics. *Acta Crystallogr D Biol Crystallogr* **60**, 2126-2132, doi:10.1107/S0907444904019158 (2004).
34 Smart, O. S., Neduvelil, J. G., Wang, X., Wallace, B. A. & Sansom, M. S. HOLE: a program for the analysis of the pore dimensions of ion channel structural models. *J Mol Graph* **14**, 354-360, 376 (1996).
35 Alexander, N., Woetzel, N. & Meiler, J. bcl::Cluster : A method for clustering biological molecules coupled with visualization in the Pymol Molecular Graphics System. *IEEE Int Conf Comput Adv Bio Med Sci* **2011**, 13-18, doi:10.1109/ICCABS.2011.5729867 (2011).

ACKNOWLEDGEMENTS

We thank Dr. Ji-fang Zhang and Dr. AjaySingh Tanwar at Thomas Jefferson University for the gift of purified rat calmodulin. We thank Denice Major for assistance with hybridoma and cell culture at Department of Ophthalmology and Visual Sciences (supported by the National Institutes of Health Core Grant P30EY11373). We acknowledge the use of instruments at the Electron Imaging Center for NanoMachines supported by NIH (1S10RR23057 and 1S10OD018111), NSF (DBI-1338135) and CNSI at UCLA. This work was supported by grants from the National Institute of Health (R01GM103899 to V.Y.M.-B., U24 GM116792 to Z.H.Z and V.Y.M.-B). We also acknowledge microscopist Carol Bator and the use of instrument at the Penn State Cryo Electron Microscopy Facility (University Park, PA). We thank Dr. David Lodowski at Case Western Reserve University for help in the early stage of the project.

AUTHORS CONTRIBUTIONS

T.E.T.H. conducted all biochemical and cryo-EM studies, including protein purification, sample preparation, cryo-EM data collection, data analysis and interpretation; R.A.P. built and refined all atomic models; E.C.F.

assisted T.E.T.H. and R.A.P. in data analysis; K.W.H. assisted T.E.T.H. in cryo-EM data collection; A.S. and S.M. trained and assisted T.E.T.H. in cryo-EM sample preparation and screening; Z.H.Z. supervised cryo-EM data collection; V.Y.M-B. designed and supervised the execution of all experiments in this manuscript; T.E.T.H. drafted the manuscript; T.E.T.H., R.A.P. and V.Y.M.-B. wrote the final version of the manuscript; All authors contributed to and reviewed the final manuscript.

	Lipid-Bound TRPV5	CaM-Bound TRPV5 C1 symmetry	CaM-Bound TRPV5 C4 symmetry
Data collection and processing			
Magnification	45,455	59,000	59,000
Voltage (kV)	300	300	300
Defocus range (μm)	1.0-2.5	1.0-2.5	1.0-2.5
Pixel size (Å)	0.55	1.14	1.14
Symmetry imposed	C4	C1	C4
Initial particle images (no.)	>1.5 million	406,838	406,838
Final particle images (no.)	50,566	45,950	45,950
Map resolution (Å)	3.9	6.2	4.9
FSC threshold	0.143	0.143	0.143
Map resolution range (Å)	3.0-4.5	5.0-7.0	3.0-5.0
Refinement			
Model resolution cut-off (Å)	3.9	6.2	4.9
FSC threshold	0.143	0.143	0.143
Map sharpening *B* factor (Å^2)	-174	-296	-290
Model composition			
Nonhydrogen atoms	2	2	0
Protein residues	2442	2595	2442
Ligands	28	16	16
R.m.s. deviations			
Bond lengths (Å)	0.006	0.005	0.005
Bond angles (°)	1.18	1.30	1.16
Validation			
MolProbity score	1.55	1.21	1.56
Clashscore	4.91	1.28	4.77
Poor rotamers (%)	0.00	0.00	0.00
Ramachandran plot			
Favored (%)	95.72	94.73	95.56
Allowed (%)	4.28	5.63	4.44
Disallowed (%)	0.00	0.00	0.00

Figure 1

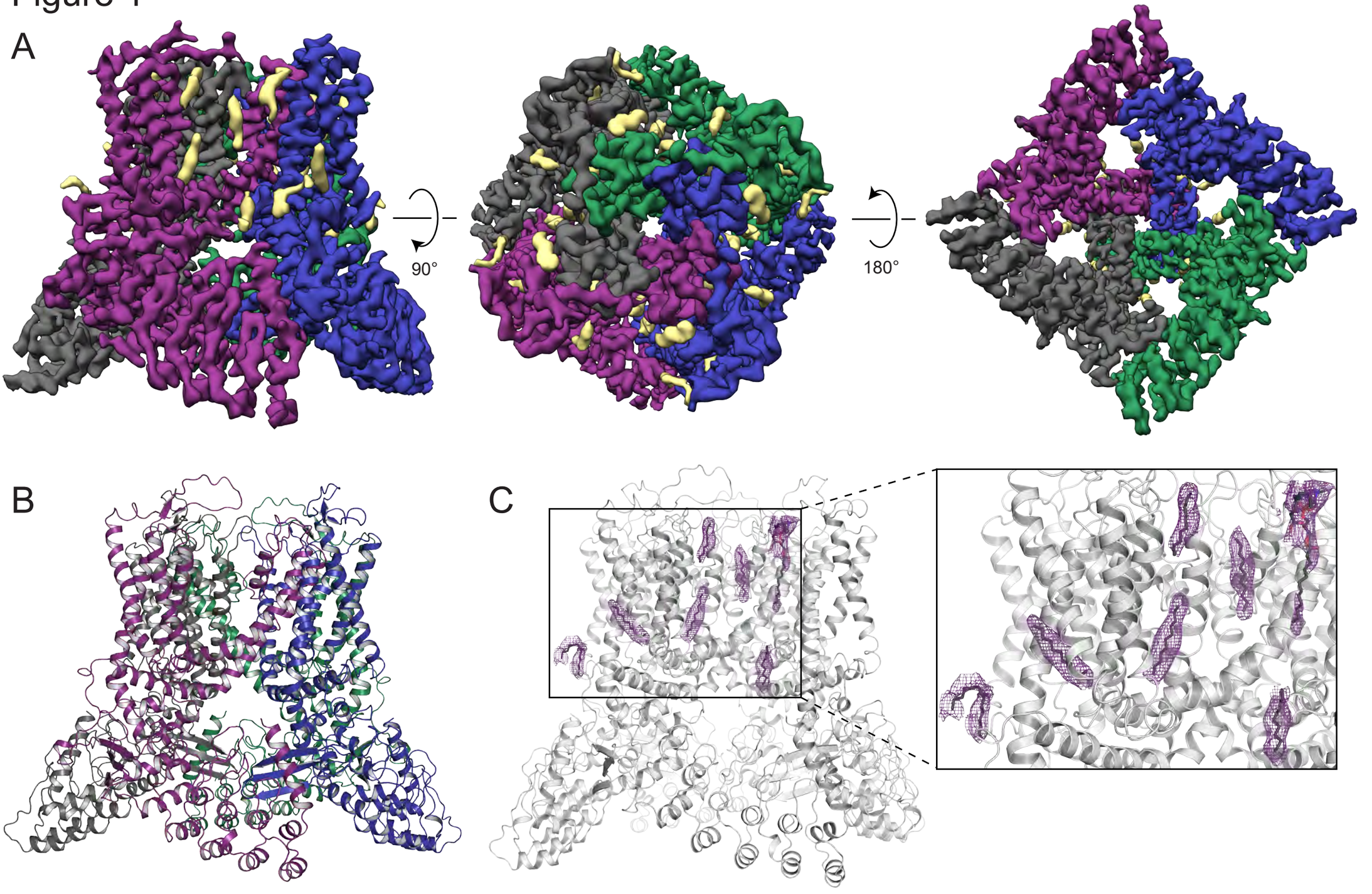

Figure 1. Lipid-bound TRPV5 structure as determined by cryo-EM. (**a**) Density map of lipid-bound TRPV5 at 3.9Å resolution. Each monomer is depicted in a different color and the densities attributed to annular lipids are shown in khaki. (**b**) Cartoon representation of the lipid-bound TRPV5 model. Each monomer is shown in a different color. (**c**) Cartoon representation of the lipid-bound TRPV5 model in grey with the seven non-protein densities per monomer attributed annular lipids shown in purple mesh and sticks.

Figure 2

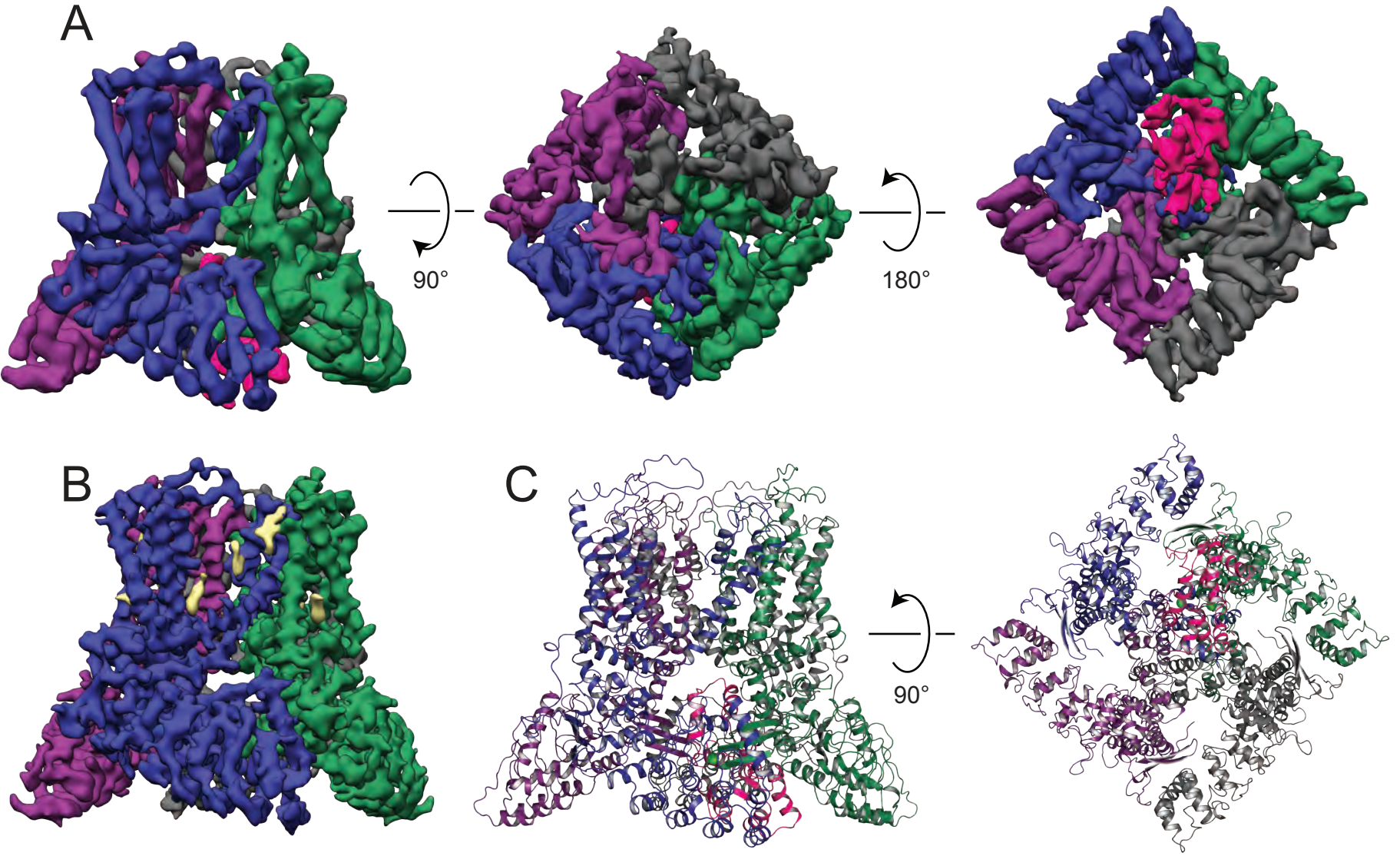

Figure 2. Calmodulin (CaM) bound TRPV5 structure as determined by cryo-EM. (**a**) Density maps of CaM-bound TRPV5 without applied symmetry refinement at 6.2Å. Each monomer is depicted in a different color and the density attributed to CaM is shown in hot pink. (**b**) CaM-bound TRPV5 refined with C4 symmetry at 4.9Å. Non-protein densities attributed to lipids are shown in khaki. (**c**) Final CaM-bound TRPV5 model refined against the C1 symmetry map. Calcium ions are depicted as green spheres.

Figure 3

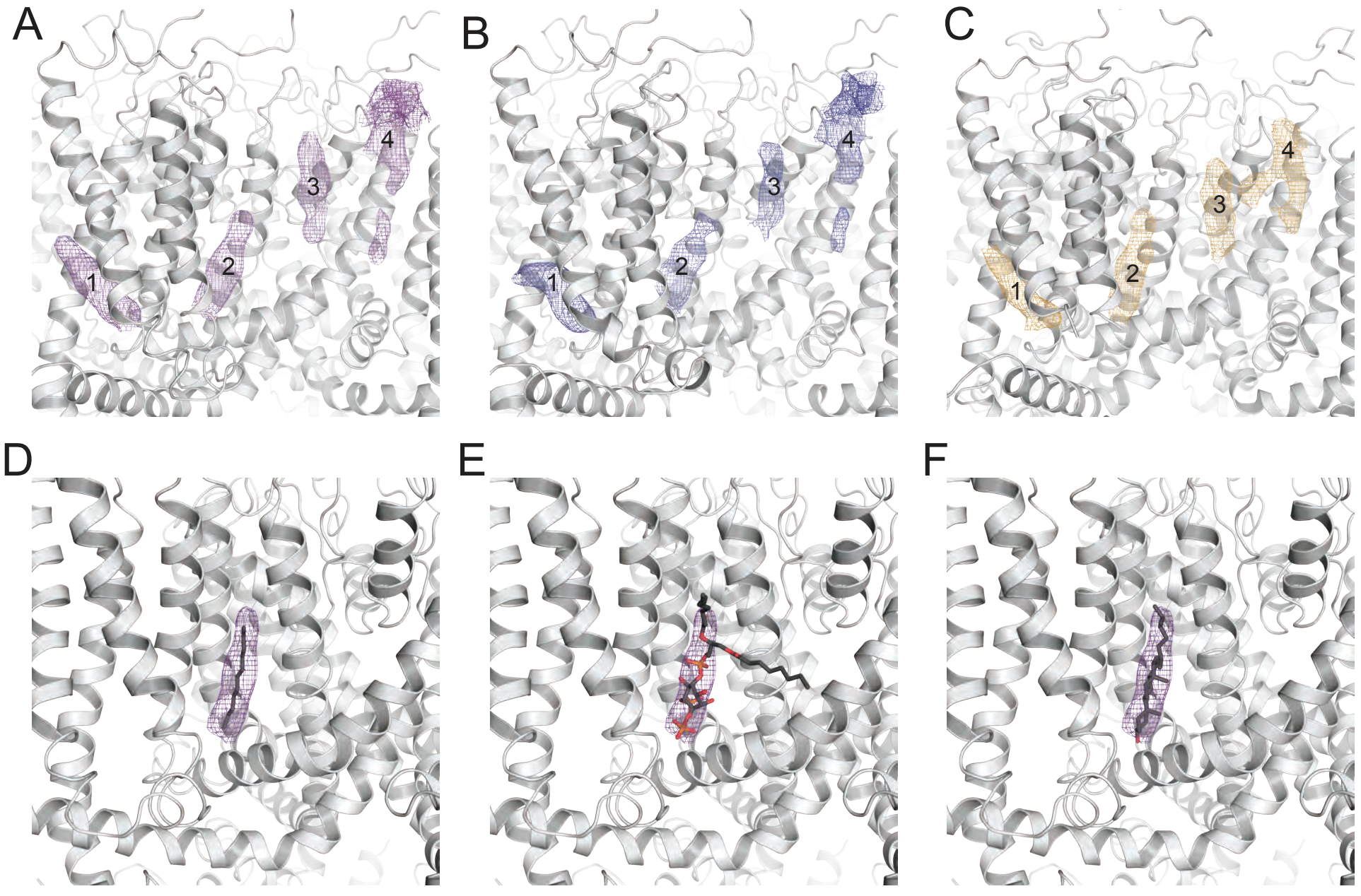

Figure 3. Conserved lipid densities. (**a**) A close-up view of the TMD of the lipid-bound TRPV5 model. Four high confidence lipid densities are shown in purple mesh. As the identity of the lipids are unclear they have been labeled as Lipid1-4. (**b**) A close-up view of the TMD of the CaM-bound TRPV5 model. Four high confidence lipid densities are shown in blue mesh and labeled as Lipids 1-4. (**c**) The TMD of the human TRPV6 structure in nanodiscs (PDB 6BO8). Four strong lipid densities are shown in orange mesh. (***d***) diC8 (grey sticks) docked to the Lipid 2 density (purple mesh). (**e**) PI(4,5)P2 diC8 (grey sticks) docked to the Lipid 2 density (purple mesh). (**f**) Cholesterol (grey sticks) docked to the Lipid 2 density.

Figure 4

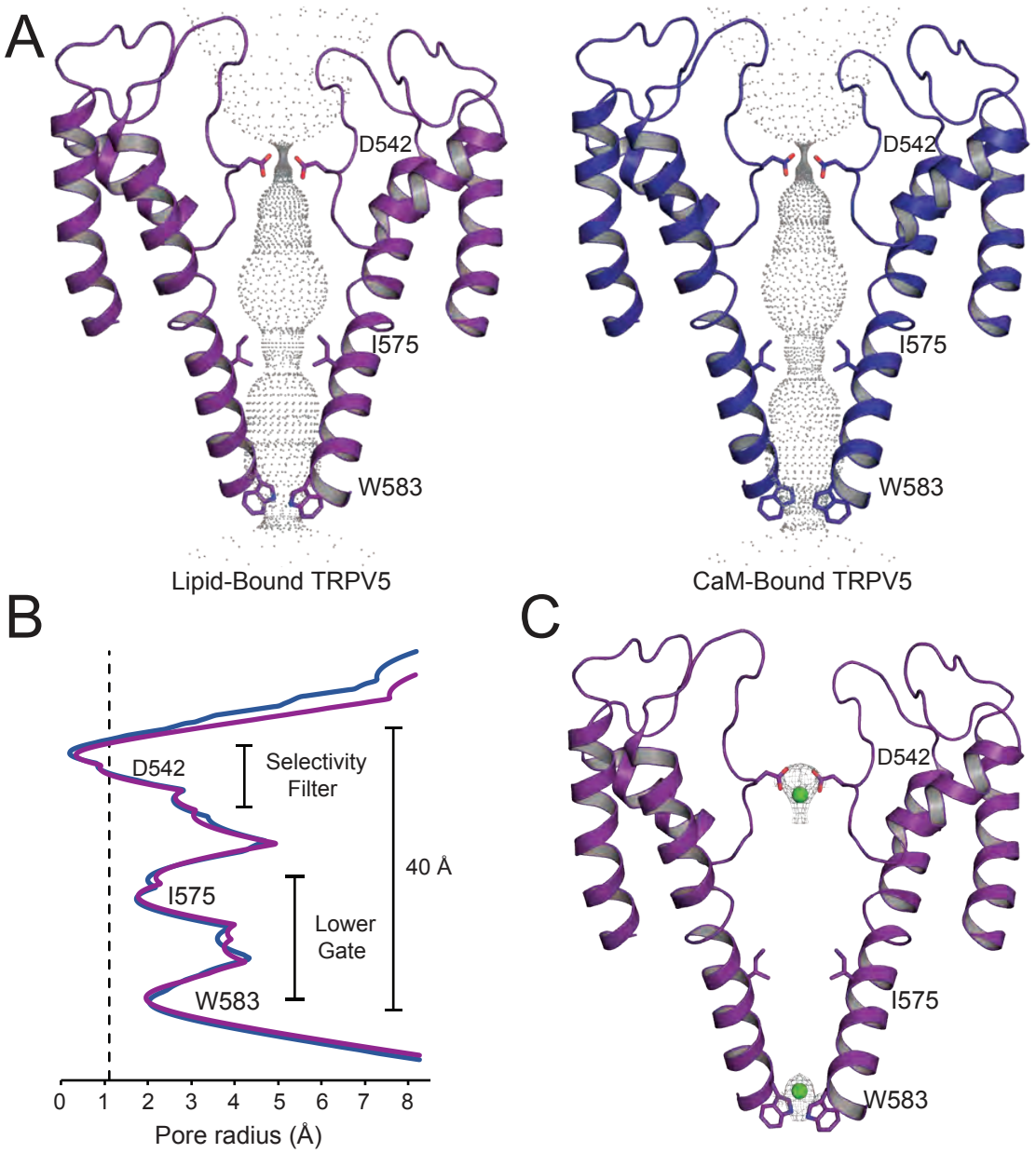

Figure 4. Pore comparison of lipid-bound and CaM-bound TRPV5. (**a**) Lipid-bound TRPV5 pore diagram (left). CaM-bound TRPV5 pore diagram (right). Constriction residues are shown as sticks. (**b**) Plot of pore radii of lipid-bound TRPV5 (purple) and CaM-bound TRPV5 (blue) as a function of distance through the pore. The dotted line indicates the radius of a calcium ion. (**c**) Lipid-bound TRPV5 pore highlighting two calcium ions found at the selectivity filter and the lower gate.

Figure 5

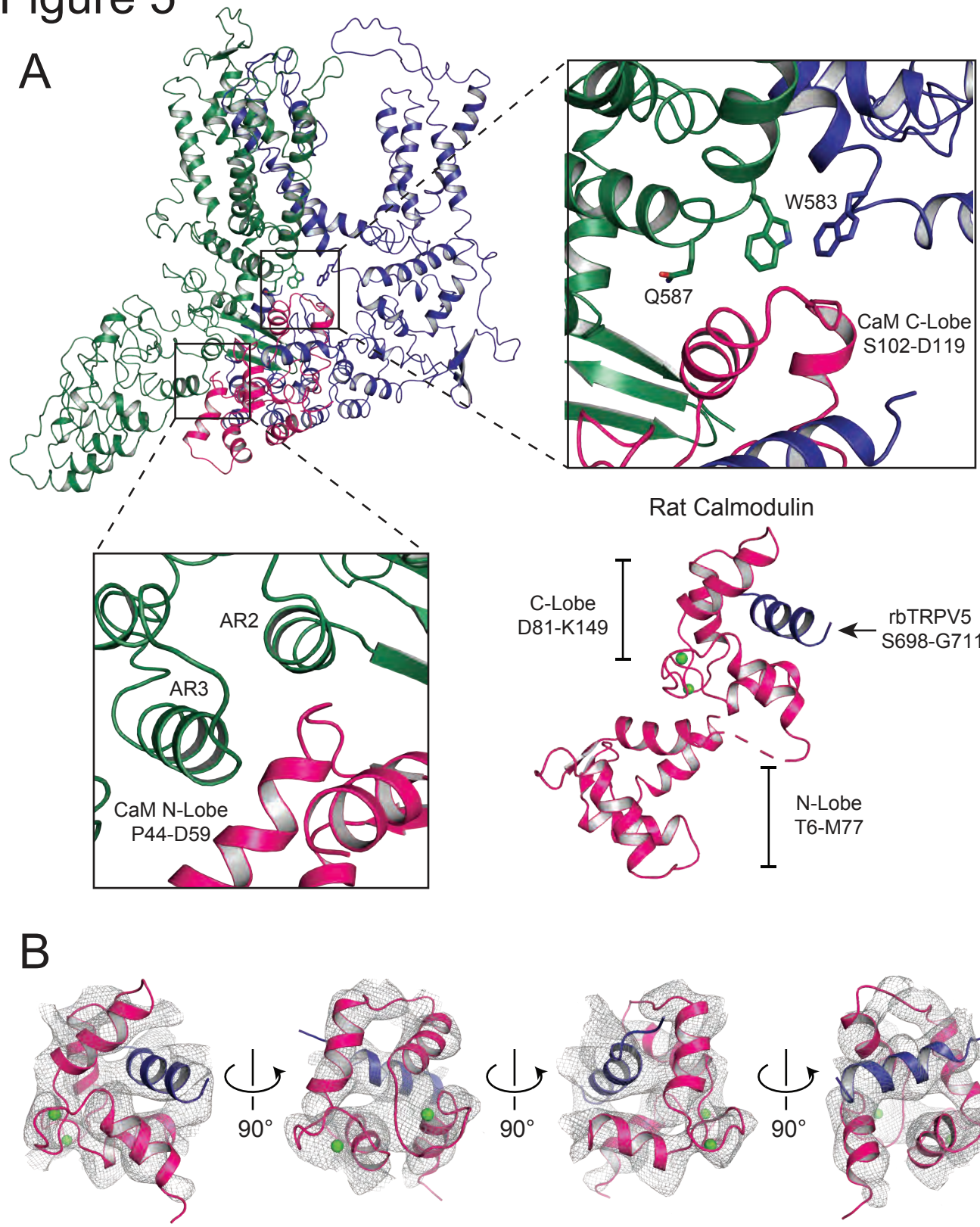

Figure 5. CaM interactions with TRPV5. (**a**) Cartoon representation of two adjacent dimers of TRPV5 (green and blue) bound to a single molecule of CaM (pink). The zoomed in views depict the interaction of CaM with TRPV5 at the pore (top right) and the ARD (bottom left). A cartoon representation of activated CaM bound to the distal C-terminus of TRPV5 with the N- and C- lobes labeled (bottom right). Residues of interest are labeled and shown as sticks. (**b**) Multiple views of the model of the CaM C-lobe (pink) fitted into the corresponding cryo-EM density (grey mesh). Calcium ions are shown as green spheres.

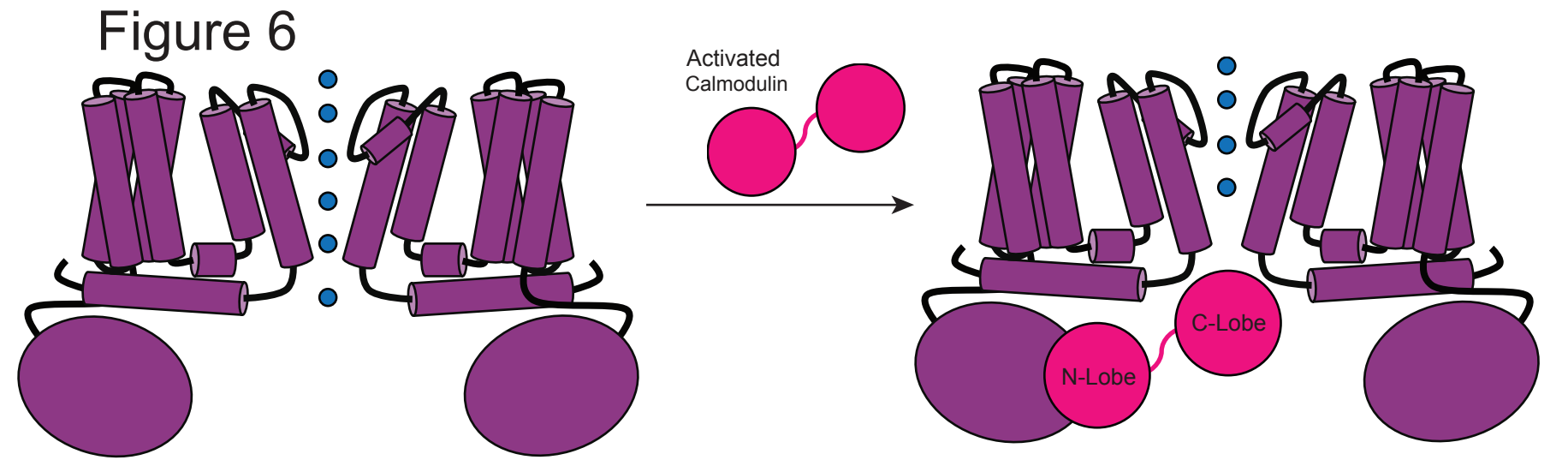

Figure 6. CaM inhibition of TRPV5. A schematic representation of the proposed binding of CaM to TRPV5 and channel inhibition mechanism. A dimer of TRPV5 is shown as a purple diagram, CaM is shown in pink and the blue circles indicate the flow of calcium ions.